energy&fuels

Article

pubs.acs.org/EF

# Hydrothermal Liquefaction Biocrude Compositions Compared to Petroleum Crude and Shale Oil

Jacqueline M. Jarvis,[†] Justin M. Billing,[‡] Richard T. Hallen,[‡] Andrew J. Schmidt,[‡] and Tanner M. Schaub*[,†]

[†]Chemical Analysis and Instrumentation Laboratory, College of Agricultural, Consumer and Environmental Sciences, New Mexico State University, 945 College Avenue, Las Cruces, New Mexico 88003, United States

[‡]Chemical and Biological Processes Development Group, Pacific Northwest National Laboratory, P.O. Box 999, Richland, Washington 99352, United States

Supporting Information

**ABSTRACT:** We provide a direct and detailed comparison of the chemical composition of petroleum crude oil (from the Gulf of Mexico), shale oil, and three biocrudes (i.e., clean pine, microalgae *Chlorella* sp., and sewage sludge feedstocks) generated by hydrothermal liquefaction (HTL). Ultrahigh resolution Fourier transform ion cyclotron resonance mass spectrometry (FT-ICR MS) reveals that HTL biocrudes are compositionally more similar to shale oil than petroleum crude oil and that only a few heteroatom classes (e.g., $N_1$, $N_2$, $N_1O_1$, and $O_1$) are common to organic sediment- and biomass-derived oils. All HTL biocrudes contain a diverse range of oxygen-containing compounds when compared to either petroleum crude or shale oil. Overall, petroleum crude and shale oil are compositionally dissimilar to HTL oils, and >85% of the elemental compositions identified within the positive-ion electrospray (ESI) mass spectra of the HTL biocrudes were not present in either the petroleum crude or shale oil (>43% for negative-ion ESI). Direct comparison of the heteroatom classes that are common to both organic sediment- and biomass-derived oils shows that HTL biocrudes generally contain species with both smaller core structures and a lower degree of alkylation relative to either the petroleum crude or the shale oil. Three-dimensional plots of carbon number versus molecular double bond equivalents (with observed abundance as the third dimension) for abundant molecular classes reveal the specific relationship of the composition of HTL biocrudes to petroleum and shale oils to inform the possible incorporation of these oils into refinery operations as a partial amendment to conventional petroleum feeds.

## INTRODUCTION

For economic, political, and environmental reasons, the development of alternative fuel sources has become imperative, and the generation of liquid fuels derived from biomass is widely sought. Biomass provides hydrocarbon-rich molecules composed of carbohydrates, lignin, proteins, and lipids, all of which can be converted to fuel precusrors.[1,2] Hydrothermal liquefaction (HTL) is a favorable thermochemical biomass conversion process for wet biomass feedstocks.[2,3] The ability to convert high-moisture biomass into liquid fuels without extensive drying makes HTL less energy intensive and therefore more economically viable than other thermochemical conversion techniques (e.g., pyrolysis).[3] Ultimately, HTL presents an opportunity to utilize a range of biomass feedstocks (e.g., algae, industrial wastes, and sewage sludge) to produce cost-effective, nonpetroleum fuel precursors.

Through the HTL process, elevated temperature (280−370 °C) and pressure (10−25 MPa) convert a biomass slurry (∼5−35% dry solids) into a hydrocarbon-rich oil biocrude.[1−3] Auspicious biocrude yields of 35−64 wt % and energy recoveries of 60−78% have been reported.[3] Ideally, HTL biocrude would be used as an amendment to petroleum in refinery operations to alleviate the demand for conventional fuels. However, biocrudes generally have high oxygen content (5−18%) and potentially high nitrogen content (0.3−8%), depending on feedstock[3] that render this material largely immiscible with conventional petroleum fuels, and biocrude must be upgraded independently.

Heterogeneous catalytic hydroprocessing is the forerunner for biocrude upgrading. Hydrodesulfurization from petroleum refining has been replaced with hydrodeoxygenation to reduce the oxygen content of wood HTL biocrudes to near zero.[3] Additionally, catalytic hydrodeoxygenation, hydrodenitrogenation, and hydrodesulfurization have been shown to reduce the heteroatom content of microalgae-derived biocrude to 1−2% oxygen, <0.25% nitrogen, and <50 ppm sulfur.[4] After upgrading, these hydrotreated oils can be further processed into petroleum-like products (e.g., kerosene, gasoline, diesel, jet fuel, etc.) in refineries without modifications to the existing infrastructure.[4]

Here, two petroleum standards from the National Institute of Standards and Technology (i.e., Gulf of Mexico (GOM) crude oil (SRM 2779) and shale oil (SRM 1580)) along with three HTL biocrudes derived from clean pine, *Chlorella* sp., and sewage sludge feedstocks are characterized by Fourier transform ion cyclotron resonance mass spectrometry (FT-ICR MS) for the direct comparison of the chemical composition of petroleum crude oil (i.e., geologically mature oil), shale oil (i.e., less geologically mature than petroleum), and HTL biocrudes

Received: November 14, 2016
Revised: January 18, 2017
Published: February 7, 2017






DOI: 10.1021/acs.energyfuels.6b03022
Energy Fuels 2017, 31, 2896−2906

Table 1. Properties of Biocrudes Derived from Pine, *Chlorella* sp., and Sewage Sludge Feedstocks and Typical Elemental Ranges[30] for Petroleum

| | pine | *Chlorella* sp. | sewage sludge | petroleum[d] |
|---|---|---|---|---|
| carbon (wt %)[a] | 83% | 79% | 77% | 83−87% |
| hydrogen (wt %)[a] | 6.7% | 10.6% | 10.1% | 10−14% |
| oxygen (wt %)[a,c] | 10.0% | 3.7% | 8.1% | 0.05−1.5% |
| nitrogen (wt %)[a] | 0.2% | 5.5% | 4.3% | 0.1−2% |
| sulfur (wt %)[a] | 0.0% | 0.6% | 0.6% | 0.05−6% |
| H:C (mol ratio)[a] | 0.97 | 1.60 | 1.57 | |
| HHV (MJ/kg)[a] | 35.9 | 39.6 | 37.8 | |
| TAN (mg KOH/g oil)[b] | 53 | 53 | 65 | |
| density (g/mL)[b] | 1.10 | 0.96 | 1.00 | |
| viscosity (cSt@40 °C)[b] | >10,000 | 295 | 571 | |
| moisture (wt %)[b] | 16.9% | 12.0% | 13.0% | |
| ash (wt %)[b] | 0.07% | 0.47% | 0.33% | |
| filterable solids (wt %)[b] | 0.04% | 0.36% | 0.18% | |

[a]Dry basis. [b]Whole oil. [c]By difference. [d]From ref 30.

(i.e., derived from fresh biomass sources). FT-ICR mass spectrometry has been used to identify tens of thousands of compounds present within petroleum crude oils, and these data can be used to predict both value and behavior.[5−12] A "petroleomic" correlation between oil behavior/properties and chemical composition can also be applied to biocrude. Characterization of forest pine residual and microalgal HTL biocrudes by FT-ICR MS has been performed previously, but a direct correlation to the composition of petroleum has not been attempted previously.[13−16] Recently, metal-containing porphyrin compounds found within both petroleum crude oil and HTL biocrudes have been reported to cause similar issues in hydroprocessing units.[17−20] Here, we directly compare the chemical composition of HTL biocrudes to GOM crude oil and shale oil, with a single and powerful analytical platform, to determine the compositional overlap between these oils.

## METHODS

**Samples.** Gulf of Mexico (GOM) crude oil (Standard Reference Material (SRM) 2779) and shale oil (SRM 1580) were obtained from the National Institute of Standards and Technology (NIST). Biocrude samples were obtained from the hydrothermal liquefaction of pine, *Chlorella* sp., and sewage sludge performed at Pacific Northwest National Laboratory (PNNL). The HTL biocrudes characterized in this paper were generated in continuous flow bench scale reactor systems operated at liquid hourly space velocities of 2 to 4 L/L/h, temperatures 345 ± 5 °C, and pressures 2900 ± 50 psig.[4,21] The biocrude samples are recovered as a separate phase from the largely aqueous product; no solvents are used for product recovery. Pine feedstock was obtained as wood flour from Idaho National Laboratory. *Chlorella sp*. feedstock was obtained from Global Algae Innovations (http://www.globalgae.com). The sewage sludge biocrude sample was prepared from primary sewage sludge provided by Metro Vancouver WWTP.[21,22] The total solids and ash contents of the slurry feeds on a total slurry basis were as follows: 13.5 wt %-solids, 1.1 wt %-ash for clean pine; 22.1 wt %-solids, 3.1 wt %-ash *Chlorella* sp.; and 11.9 wt %-solids, 0.9 wt %-ash for primary sewage sewage sludge.

**Analysis of Biocrude Properties.** The HTL biocrude samples were analyzed for CHN (ASM D5373/D5291), S (ASTM D4239/D1552), moisture (Karl Fisher analysis, ASTM D6869), and total acid number (mg KOH/g; ASTM D3339) (Table 1). Oxygen was determined by difference. Trace element analysis was conducted via ICP-OES as described previously (Table S1).[4]

**Sample Preparation and Ionization for Mass Spectrometry.** The GOM and the shale oils were dissolved in toluene (HPLC grade, JT Baker, Phillipsburg, NJ), and biocrudes were dissolved in 1:1 chloroform:methanol (HPLC grade, JT Baker, Phillipsburg, NJ) to create 1 mg/mL stock solutions. Final samples were further diluted in methanol (HPLC grade, JT Baker, Phillipsburg, NJ) to 250 μg/mL 1% formic acid (Fluka Analytical, St. Louis, MO) for positive-ion electrospray ionization (ESI). For negative-ion ESI, 0.25% (v/v) tetramethylammonium hydroxide (TMAH) solution (25 wt % in MeOH, Acros Organics, Fair Lawn, NJ) was added to the GOM and shale oils, and 0.0625% TMAH solution was added to biocrude samples to aid in deprotonation of ions. Stock solutions were diluted to a final sample concentration of 100 μg/mL in 90:10 methanol:toluene (biocrudes) or 100% toluene (petroleum) for positive-ion atmospheric pressure photoionization (APPI).

For electrospray ionization, a syringe pump delivered the samples to the ionization source at a rate of 0.5 μL/min, and 2.5 kV was applied to the ESI needle. Atmospheric pressure photoionization (APPI) was performed with an Ion Max APPI source (ThermoFisher Corp., San Jose, CA). Samples were introduced to the source through a fused silica capillary at a rate of 50 μL/min. Nitrogen was used as a sheath gas (60 psi) and auxiliary gas (4 L/min). Inside the heated vaporizer of the source (~300 °C), the sample is mixed with a nebulization gas ($N_2$) and is passed under a krypton VUV lamp producing 10 eV photons (120 nm). Toluene was added to the samples to increase ionization efficiency through dopant-assisted photoionization.

**Mass Spectrometry.** Samples were analyzed with a custom-built 9.4 T Fourier transform ion cyclotron resonance mass spectrometer at the national FT-ICR MS user facility at the National High Magnetic Field Laboratory.[23] Data collection was facilitated by a modular ICR data acquisition system (PREDATOR).[24] Ions generated at atmospheric pressure were introduced into the mass spectrometer via a heated metal capillary. Ions were guided through the skimmer region (~2 Torr) and allowed to accumulate in the first octopole (rf-only) for ESI.[25] Ions were sent through the quadrupole (mass transfer mode) to a second octopole where the ions were collisionally cooled for 1 ms with helium gas (~(4−5) × $10^{-6}$ Torr at gauge) before passage through a transfer octopole to the ICR cell (open cylindrical Penning trap[26]). For APPI, ions were allowed to pass directly through the first octopole and quadrupole for accumulation in the second octopole prior to transfer to the ICR cell.

Multiple (50) individual time-domain transients were coadded, Hanning-apodized, zero-filled, and fast Fourier transformed prior to frequency conversion to mass-to-charge ratio[27] to obtain the final mass spectrum. The time domain signal acquisition period was ~5.6−6.9 s. All observed ions were singly charged, as evident from unit $m/z$ spacing between species which differ by $^{12}C_c$ vs $^{13}C_1{}^{12}C_{c-1}$.

**Data Analysis and Visualization.** Data were analyzed, and peak lists were generated with PetroOrg software.[28] Internal calibration of the spectrum was based on homologous series whose elemental compositions differ by integer multiples of 14.01565 Da (i.e., $CH_2$).[29] The peaks within the mass spectrum are represented as a relative abundance of the base peak in the mass spectrum, which is 100%.



DOI: 10.1021/acs.energyfuels.6b03022
*Energy Fuels* 2017, 31, 2896−2906

Data are visualized by relative abundance histograms for heteroatom classes (i.e., grouped by the composition of heteroatoms per molecule not including carbon and hydrogen and abbreviated as such) with a sum greater than 5% relative abundance and from isoabundance-contoured plots of double bond equivalents (DBE = number of rings plus double bonds to carbon) vs carbon number for members of a single heteroatom class. The relative abundance scale in isoabundance-contoured plots is scaled relative to the most abundant species in that class.

## RESULTS AND DISCUSSION

**Elemental Analysis and Heteroatom Class Distributions.** As noted by Speight, the elemental composition of petroleum falls into a very narrow range, regardless of source.[30] Carbon (83−87%) and hydrogen (10−14%) are the most abundant elements in petroleum and account for >93 wt %. The remainder of the petroleum is comprised mostly of nitrogen (0.1−2%), oxygen (0.05−1.5%), and sulfur (0.05−6%). In general, conventional crude oil contains <0.5% nitrogen, <0.5% oxygen, and <2% sulfur.[30]

In comparison, the carbon (∼77−83%) and hydrogen (∼7−11%) contents of HTL biocrudes are similar but slightly lower than petroleum due to higher concentrations of heteroatoms in biocrudes (Table 1). HTL biocrudes have higher oxygen contents than petroleum, which range from 3.7% in *Chlorella* sp. biocrude and up to 8.1% and 10.0% in sewage sludge and pine biocrudes (Table 1). The pine HTL biocrude has a lower sulfur content (i.e., not detectable) than petroleum, and its nitrogen content (0.2%) is at the low end of the range in petroleum. In contrast, the sewage sludge and *Chlorella* sp. biocrudes have significantly higher nitrogen contents (∼4−6%) than petroleum and contain ∼0.6% sulfur, which is within the range for petroleum. The higher heteroatom contents result in increased heteroatom class complexity of HTL biocrudes relative to petroleum.

Heteroatom classes present in the greatest relative abundance in petroleum crude oil are characterized by a few heteroatoms (typically ≤4 heteroatoms) and low oxygen content ($O \leq 4$)[5,17] whereas HTL biocrudes contain significantly higher oxygen and sometimes nitrogen (i.e., sewage sludge and *Chlorella* sp. biocrudes) contents ($0 \leq N \leq 6$, $0 \leq O \leq 15$, $0 \leq S \leq 1$). Figure 1 shows the heteroatom class distributions derived from the (+) ESI FT-ICR mass spectra of GOM crude oil, shale oil, pine, *Chlorella* sp., and sewage sludge. The crude oils derived from organic sediments (i.e., GOM and shale oils) contain a high relative abundance of $N_1$, $N_2$, and $N_1O_x$ (predominately $N_1O_1$) species, whereas the HTL biocrudes (i.e., pine, *Chlorella* sp., and sewage sludge) are characterized by heteroatom classes with higher oxygen contents ($O > 4$). The *Chlorella* sp. and sewage sludge HTL biocrude contain higher contents of nitrogen than the pine biocrude, thus they have a higher relative abundance of nitrogen-containing classes whereas the pine biocrude is dominated by sodiated $O_x$ species (>60% relative abundance). Sodium carbonate is added to the pine feedstock prior to HTL to act as a buffer to keep the pH of the resulting products from going below 4[31] and is the major source of sodium in the biocrude. The *Chlorella* sp. and sewage sludge HTL biocrudes have a similar relative abundance (∼10%) of $N_2$ species as the shale oil; however, they contain a higher relative abundance of nitrogen- and oxygen-containing species (i.e., $N_{2-4}O_x$) than the shale oil. Interestingly, the biocrudes derived from *Chlorella* sp. and sewage sludge have similar heteroatom class distributions even though they are generated from different biomass sources.

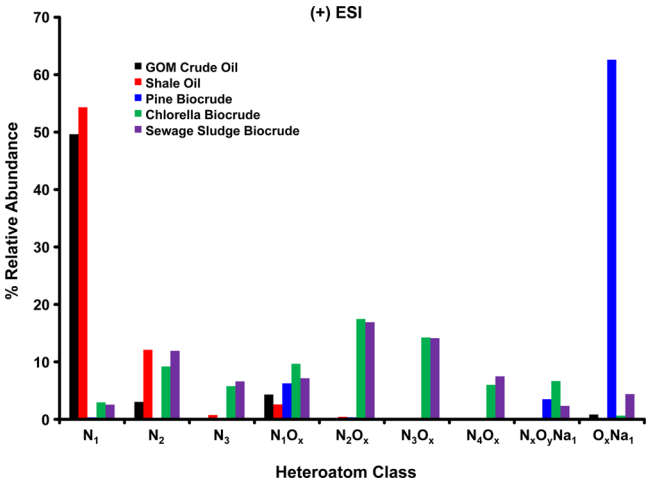


**Figure 1.** Heteroatom class distributions derived from the (+) ESI mass spectra of GOM crude oil, shale oil, pine HTL biocrude, *Chlorella* sp. HTL biocrude, and sewage sludge HTL biocrude.

The heteroatom class distributions derived from the (+) APPI FT-ICR mass spectra of GOM crude oil, shale oil, and HTL biocrudes have similar trends as seen in the positive-ion ESI heteroatom class distributions (Figure S1). The main difference from positive-ion ESI is the higher relative abundances of hydrocarbon (HC), $S_1$, and oxygen-containing species within the positive-ion APPI mass spectra of the organic sediment-derived oils due to the increased ionization efficiency of aromatic species. The GOM crude oil is comprised of HC (44%), $N_1$ (10%), $S_1$ (9%), and $O_1$ (9%) classes, whereas the shale oil contains mostly HC (7%), $N_1$ (35%), $N_2$ (10%), and $N_1O_1$ (19%) species. The *Chlorella* sp. and sewage sludge HTL biocrudes are mainly comprised of $N_{1-4}O_x$ species (∼65%), whereas the pine HTL biocrude is dominated by $O_x$ (55%) and $N_1O_x$ (20%) species. Importantly, positive ion mode heteroatom class distributions show more sulfur-containing compounds (mainly $S_1$ species) in the organic sediment-derived oils than the HTL biocrudes. Sulfur-containing compounds were not detected in the pine biocrude as expected (i.e., sulfur not detected in elemental analysis). However, the *Chlorella* sp. and sewage sludge biocrudes have sulfur contents (∼0.6%) similar to petroleum-derived oils, thus sulfur-containing compounds would be expected in these biocrudes. Interestingly, the sulfur-containing species within these biocrudes are mostly $N_xO_yS_1$ in the *Chlorella* sp. biocrude and $N_xO_yS_1$ and $O_xS_1$ species in the sewage sludge biocrude (all classes present in ≤0.1% relative abundance and represent <0.5% of the total relative abundance) and not $S_1$ species detected in organic sediment-derived oils. Additionally, the heteroatom class distributions derived from the (−) ESI FT-ICR mass spectra of GOM crude oil, shale oil, and HTL biocrudes also show notable differences in heteroatom class composition based upon source material (Figure 2). The GOM crude oil is comprised mostly of HC, $N_1$, $N_1O_x$, and $O_x$ species, while the shale oil contains these same classes in addition to $N_2$ and $N_2O_x$ species. Similar to the positive-ion ESI results, the negative-ion ESI mass spectrum of pine HTL biocrude is dominated by $O_x$ species (∼78%). The negative-ion ESI mass spectra of *Chlorella* sp. and sewage sludge HTL biocrudes contain a higher relative abundance of $O_x$ species (∼37% and 28%), predominately from fatty acids, and fewer nitrogen atoms


DOI: 10.1021/acs.energyfuels.6b03022
Energy Fuels 2017, 31, 2896−2906

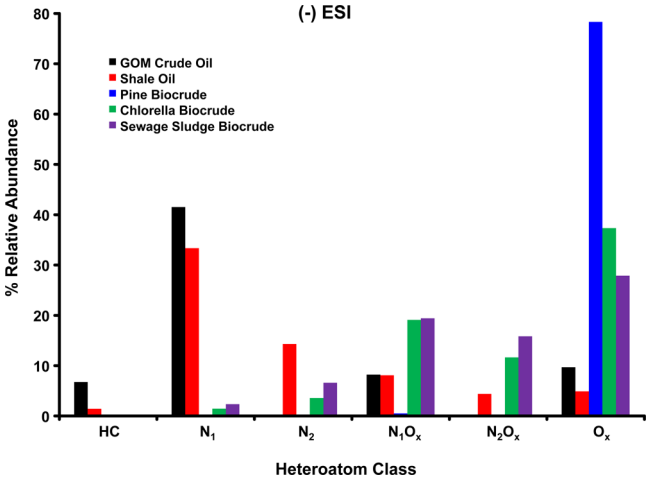


**Figure 2.** Heteroatom class distributions derived from the (−) ESI mass spectra of GOM crude oil, shale oil, pine HTL biocrude, *Chlorella* sp. HTL biocrude, and sewage sludge HTL biocrude.

per molecule ($N < 3$) than the species present in the positive-ion mass spectra.

To gain a better understanding of the similarities and differences between organic sediment-derived and biomass-derived oils, the number of monoisotopic peaks assigned to (±) ESI and (+) APPI mass spectra of GOM crude oil, shale oil, and pine, *Chlorella* sp., and sewage sludge HTL biocrudes are presented in Table 2. The positive-ion mass spectra of biocrudes contain at least twice as many peaks as the organic sediment-derived oils, whereas the opposite is true for the negative-ion mass spectra. Positive-ion ESI mass spectra of the GOM crude oil and shale oil are dominated by a few highly abundant pyridinic nitrogen species (i.e., 1−2 nitrogen and oxygen atoms per molecule) which are ionized preferentially over most other species present within the samples. However, the *Chlorella* sp. and sewage sludge biocrudes contain a much broader range of pyridinic nitrogen compounds (i.e., 1−6 nitrogen and 1−7 oxygen atoms per molecule). For the positive-ion ESI mass spectrum of the pine biocrude, sodiated adducts of $O_x$ species are observed in higher abundance than nitrogen-containing species. Alternatively, the negative-ion ESI mass spectra of the *Chlorella* sp. and sewage sludge biocrudes are dominated by a few, very efficiently ionized carboxylic acid species (which decrease the dynamic range for detection of other species), whereas the GOM crude oil and shale oil contain several different functionalities (e.g., hydrocarbons, pyrrolic nitrogen, carboxylic acids, phenols) amenable to ionization by negative-ion ESI. Similar to positive-ion ESI, the $O_x$ species dominate the negative-ion ESI mass spectrum of pine biocrude; however, the $O_x$ species with carboxylic acid functionalities were far more efficiently ionized (i.e., no pyrrolic nitrogen species), thus limiting the number of species detectable by negative-ion ESI.

**Table 2. Assigned Monoisotopic Peaks from FT-ICR MS Analyses of Pine, Chlorella, and Primary Sludge Biocrudes and Gulf of Mexico (GOM) and Shale Crude Oils**

| | (+) APPI | | (+) ESI | | (−) ESI | |
|---|---|---|---|---|---|---|
| | no. of peaks | % total | no. of peaks | % total | no. of peaks | % total |
| *total pine* | *6400* | | *8539* | | *1722* | |
| pine/GOM | 339 | 5% | 288 | 3% | 254 | 15% |
| pine/shale oil | 576 | 9% | 223 | 3% | 231 | 13% |
| not in GOM or shale oils | 5660 | 88% | 8186 | 96% | 1385 | 80% |
| *total Chlorella* | *13937* | | *9829* | | *1491* | |
| Chlorella/GOM | 650 | 5% | 556 | 6% | 138 | 9% |
| Chlorella/shale oil | 1772 | 13% | 831 | 9% | 806 | 54% |
| not in GOM or shale oils | 11836 | 85% | 8834 | 90% | 672 | 45% |
| *total sewage sludge* | *12432* | | *11351* | | *1722* | |
| sewage sludge/GOM | 417 | 3% | 699 | 6% | 247 | 14% |
| sewage sludge/shale oil | 1700 | 14% | 839 | 7% | 955 | 56% |
| not in GOM or shale oils | 10694 | 86% | 10227 | 90% | 741 | 43% |
| *total GOM* | *3201* | | *3525* | | *3685* | |
| not in biocrude | 2175 | 68% | 2721 | 77% | 3250 | 88% |
| *total shale oil* | *3082* | | *1207* | | *4764* | |
| not in biocrude | 1016 | 33% | 331 | 27% | 3565 | 75% |

Table 2 also shows the number of monoisotopic elemental compositions that are common to the GOM crude oil, shale oil, and HTL biocrudes. Only 3% of the molecular formulas assigned within the pine biocrude overlap with molecular formulas within the organic sediment-derived oils. In total, 96% of the molecular formulas assigned to the positive-ion ESI mass spectra of the pine biocrude are not present in either the GOM crude oil or the shale oil. Similar results are seen for the *Chlorella* sp. and sewage sludge biocrudes. Less than 10% of the molecular formulas assigned to the positive-ion ESI mass spectra of either the *Chlorella* sp. or sewage sludge biocrudes are assigned to species from the GOM crude oil or shale oil as well. Additionally, 77% of the assigned elemental compositions observed for the positive-ion ESI mass spectrum of the GOM crude oil are not present in any of the HTL biocrudes. However, only 27% of the assigned elemental compositions observed by positive-ion ESI mass spectrum of the shale oil are not present in any of the HTL biocrudes, which suggests that HTL biocrudes are more compositionally similar to shale oil. This observation is reasonable considering that shale oil is a less mature oil and has a larger diversity of nitrogen-containing compounds than the GOM crude oil, which makes shale oil more analogous to the rapidly generated, nitrogen-containing biocrudes.

Conversely, the negative-ion ESI mass spectra of *Chlorella* sp. and sewage sludge biocrudes contain more elemental composition overlaps (54−56%) with the shale oil than seen in the positive-ion ESI mass spectra; however, their overlaps with the GOM crude oil are still low (<15%). Overall, the total number of elemental composition overlaps with the organic sediment-derived oils is significantly higher, with only 43−45% of the elemental formulas assigned to the negative-ion ESI mass spectra of *Chlorella* sp. and sewage sludge biocrudes not present in either the GOM crude oil or shale oil. Alternatively, the pine biocrude does not show good elemental composition overlap with either the GOM crude oil (9%) or the shale oil (13%) with 80% of its total assigned peaks not present in either oil. Similar to positive-ion ESI, 88% of the peaks assigned to the negative-ion ESI mass spectrum of the GOM crude oil are not present in any of the HTL biocrudes. Conversely, 75% of the peaks assigned to the negative-ion ESI mass spectrum of shale oil are not present in any of the HTL biocrudes. In general, the biomass-derived species ionized by negative-ion ESI overlap


DOI: 10.1021/acs.energyfuels.6b03022
*Energy Fuels* 2017, 31, 2896−2906

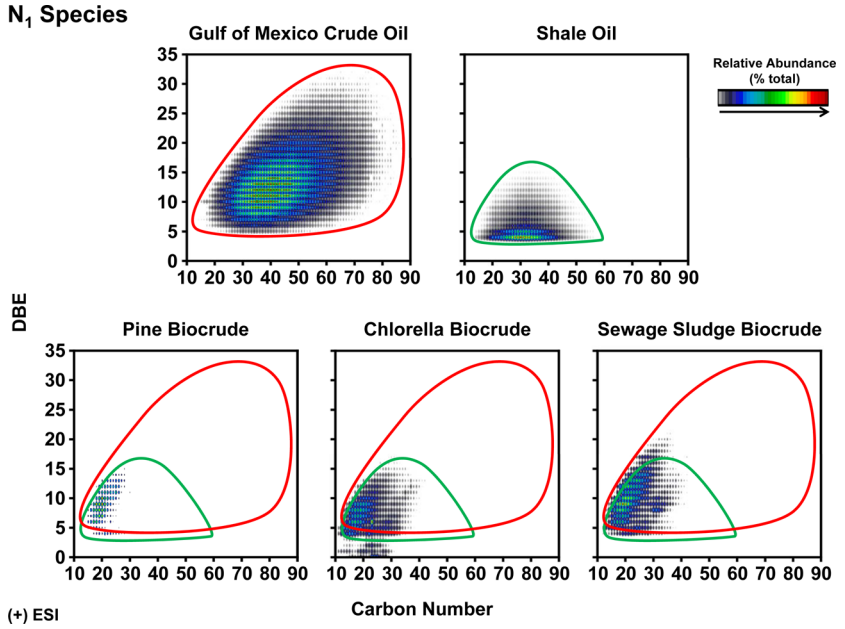


**Figure 3.** Isoabundance-contoured plots of double bond equivalents (DBE) versus carbon number for the $N_1$ species derived from the (+) ESI mass spectra GOM crude oil, shale oil, pine HTL biocrude, *Chlorella* sp. HTL biocrude, and sewage sludge HTL biocrude.

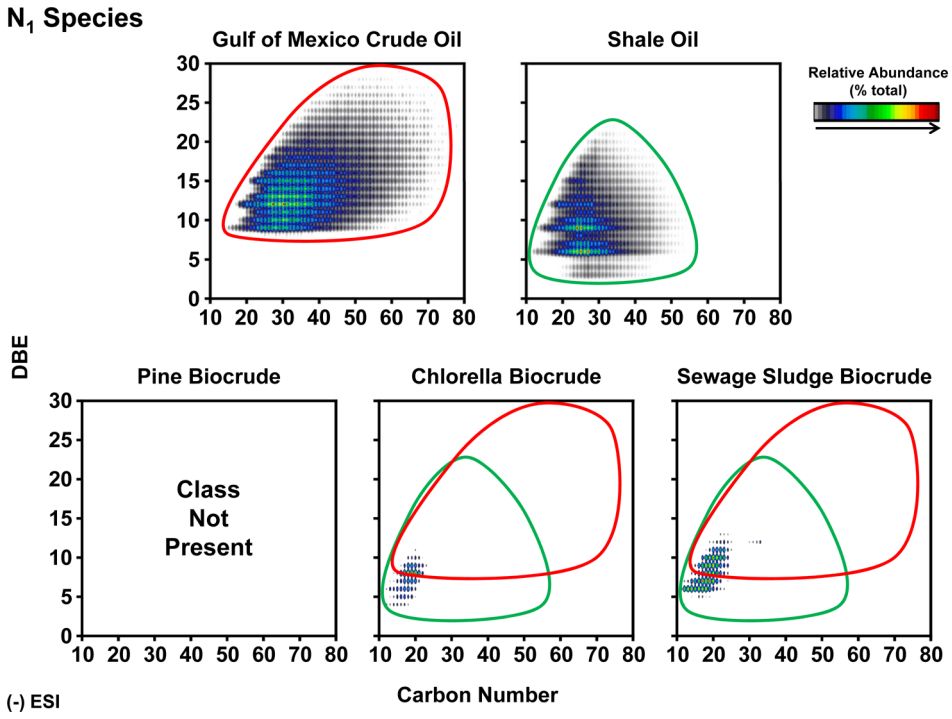


**Figure 4.** Isoabundance-contoured plots of double bond equivalents (DBE) versus carbon number for the $N_1$ species derived from the (−) ESI mass spectra GOM crude oil, shale oil, pine HTL biocrude, *Chlorella* sp. HTL biocrude, and sewage sludge HTL biocrude.

better with acidic GOM crude oil and shale oil species; however, the organic sediment-derived oils have more acidic species which are not represented in the HTL biocrudes.

**Biomass- vs Organic Sediment-Derived Compositional Space.** To further visualize the compositional space coverage of all samples, isoabundance-contoured plots of double bond equivalents (DBE = # rings + double bonds to carbon) vs carbon number for the various members of several heteroatom classes are depicted and described. We will focus on a few heteroatom classes common to GOM crude oil, shale oil, and HTL biocrude.

**$N_1$ Species.** Isoabundance-contoured plots of DBE versus carbon number for $N_1$ species observed in (+) ESI FT-ICR mass spectra of GOM crude oil, shale oil, pine HTL biocrude, *Chlorella* sp. HTL biocrude, and sewage sludge HTL biocrude are shown in Figure 3. The GOM crude oil has a broad distribution of $N_1$ species which range from $C_{15}$−$C_{87}$ and DBE 4-32 (outlined in red). The extensive variation in carbon number for any given DBE value indicates a large degree of


DOI: 10.1021/acs.energyfuels.6b03022
*Energy Fuels* 2017, 31, 2896−2906

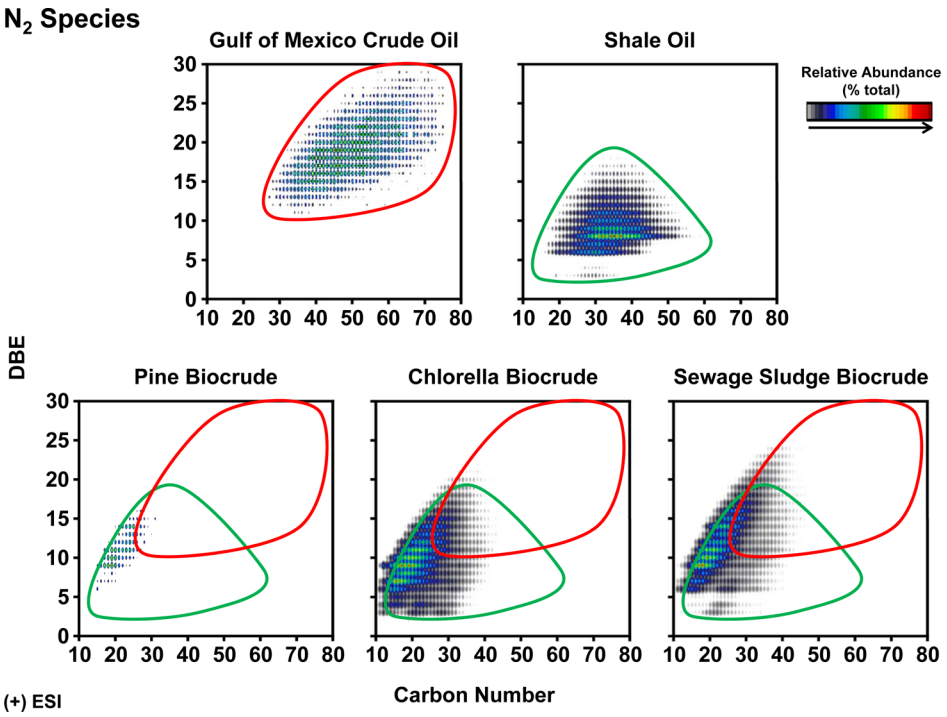


**Figure 5.** Isoabundance-contoured plots of double bond equivalents (DBE) versus carbon number for the $N_2$ species derived from the (+) ESI mass spectra GOM crude oil, shale oil, pine HTL biocrude, *Chlorella* sp. HTL biocrude, and sewage sludge HTL biocrude.

alkylation present for a given core structure. Because positive-ion ESI preferentially ionizes basic nitrogen species and the most abundance species have DBE values >4, it is implied that these species have a pyridinic nitrogen motif (Figure S2), with the addition of benzene rings (i.e., 3 additional DBE) and unsaturated side chains (or saturated rings) accounting for increases in DBE value. The most abundant basic $N_1$ species present within the GOM crude oil correlate to benzoquinoline derivatives (DBE = 10).[30,32,33] Alternatively, the $N_1$ species present in the shale oil cover a smaller compositional space than the GOM crude oil, ranging from $C_{13}$−$C_{60}$ and DBE 4-16 (outlined in green). The most abundant species in the shale oil are most likely pyridinic nitrogen derivatives (DBE = 4).[30,34] A comparison of species from organic sediment-derived sources shows that the shale oil contains less aromatic and alkylated species than the GOM crude oil.

The outlines of the organic sediment-derived species have been overlaid on the isoabundance-contoured plots of DBE vs carbon number for the members of the $N_1$ class derived from the (+) ESI FT-ICR mass spectra of HTL biocrudes to show a comparison of the compositional space coverage between the species (Figure 3). All three HTL biocrudes (i.e., pine, *Chlorella* sp., and sewage sludge) show similar compositional space coverage, indicative of similar structural motifs. The pine biocrude shows the least compositional diversity, ranging from $C_{25}$−$C_{28}$ and DBE 4-15, whereas the *Chlorella* sp. and sewage sludge biocrudes have broader compositional coverages, ranging from $C_{11}$−$C_{42}$ and DBE 0-18 for *Chlorella* sp. biocrude and $C_{11}$−$C_{42}$ and DBE 4-21 for the sewage sludge biocrude. The $N_1$ species within *Chlorella* sp. HTL biocrude appear to contain two dominant structural motifs. The nonaromatic species (DBE < 4) are most likely amine-type compounds, whereas the aromatic species (DBE > 4) correspond to compounds that contain pyridinic nitrogen.[35] The nonaromatic $N_1$ species (DBE < 4) are not present in the pine or sewage sludge biocrudes. Additionally, the *Chlorella* sp. and sewage sludge biocrudes show a higher degree of alkylation than the pine biocrude, although all three HTL biocrudes contain less alkylated species relative to the organic sediment-derived $N_1$ species, denoted by the red and green outlines. The HTL biocrude $N_1$ species fall within the lower carbon number and DBE range of the compositional space covered by organic sediment-derived $N_1$ species. Additionally, the more abundant species within HTL biocrudes are closer to the polyaromatic hydrocarbon (PAH) planar limit (Figure 3) and outside the distribution of $N_1$ species within the shale oil which indicates core structures with less alkylation are more prominent in the HTL biocrudes relative to GOM crude oil and shale oil, where a more extensive degree of alkylation is observed (e.g., abundant core structures/DBE types contain 25−40 carbon atoms per molecule).

Alternatively, the compositional space coverage for nonbasic $N_1$ species for each sample is illustrated by (−) ESI FT-ICR data for each sample in Figure 4. The GOM crude oil contains the most diverse population of nonbasic $N_1$ species, which range from $C_{15}$−$C_{78}$ and DBE 9-30. The nonbasic $N_1$ species within the GOM crude oil begin at DBE 9, which corresponds to a carbazole core structure.[30,32,33] The addition of benzene rings (i.e., addition of 3 DBE) to the carbazole structure is apparent by the higher abundance of lower carbon number species at DBE 12, 15, etc. The most abundant species are benzocarbazole homologues at DBE 12. Similar to the basic species, the nonbasic $N_1$ compounds within the GOM crude oil have the largest degree of alkylation noted by the various carbon numbers represented at any particular DBE value. In comparison, the nonbasic $N_1$ species present within the shale oil have a lower degree of alkylation, ranging from $C_{12}$−$C_{54}$, than the $N_1$ species present within the GOM crude oil. Additionally, the nonbasic species within the shale oil cover lower DBE values than those represented by the GOM crude


DOI: 10.1021/acs.energyfuels.6b03022
Energy Fuels 2017, 31, 2896−2906

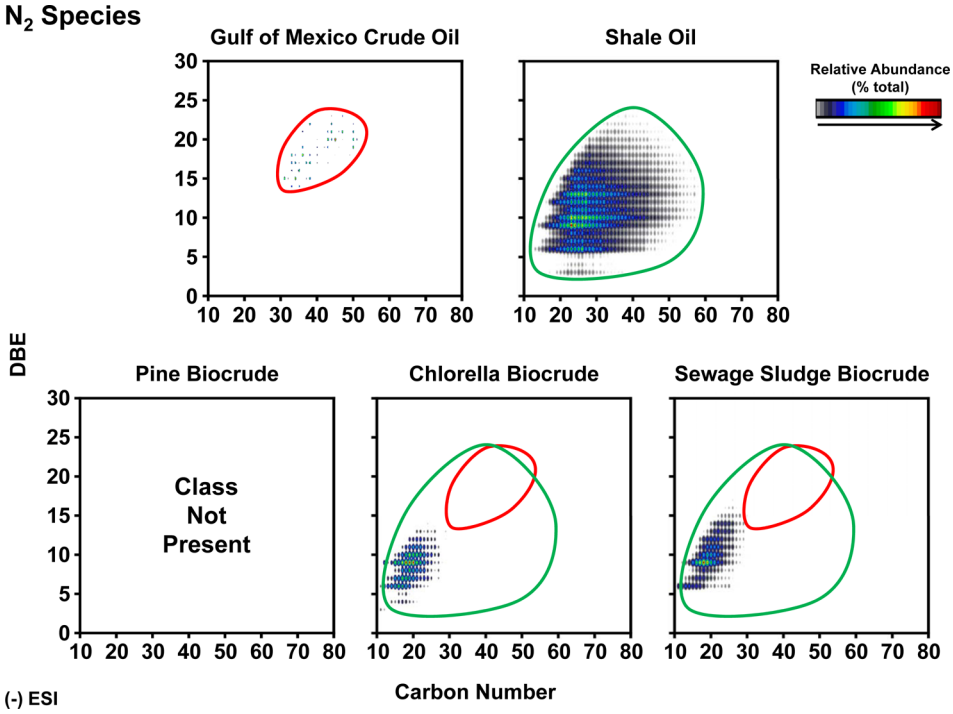


**Figure 6.** Isoabundance-contoured plots of double bond equivalents (DBE) versus carbon number for the $N_2$ species derived from the (−) ESI mass spectra GOM crude oil, shale oil, pine HTL biocrude, *Chlorella* sp. HTL biocrude, and sewage sludge HTL biocrude.

oil. The nonbasic $N_1$ species within the shale oil start at DBE 3, which corresponds to pyrrole homologues.[30,34] The addition of benzene rings to the core structure is even more apparent in the shale oil as the "hot spot" or more abundant compounds differ by 3 DBE. The most abundant core structures within the shale oil belong to indole (DBE 6) and carbazole (DBE 9) structures.

Again, the outlines of the organic sediment-derived species have been overlaid on the isoabundance-contoured plots of DBE vs carbon number for the members of the $N_1$ class derived from the (−) ESI FT-ICR mass spectra of HTL biocrudes to show a comparison of the compositional space coverage between the species (Figure 4). The nonbasic $N_1$ species present within the HTL biocrudes are significantly less diverse than the GOM crude oil and shale oil $N_1$ species. Notably, the pine HTL biocrude does not contain any nonbasic $N_1$ species. This is not surprising since the pine HTL biocrude has a very low nitrogen content. In fact, all nitrogen-containing compounds also have oxygen incorporated into the molecule for that biocrude. Alternatively, the *Chlorella* sp. and sewage sludge biocrudes do have nonbasic $N_1$ species that range from $C_{12}$−$C_{23}$ and DBE 4-11 and $C_{12}$−$C_{33}$ and DBE 5-13. The most abundant $N_1$ species within the *Chlorella* sp. HTL biocrudes have a DBE value of 8, and the lowest DBE value represented is 4. These structures do not correspond to the core pyrrole, indole, and carbazole structures present in organic sediment-derived materials. It is possible that these $N_1$ species (~1.5% relative abundance) contain more saturated rings than the fully aromatized pyrrole derivatives typically seen in (−) ESI. In contrast, the $N_1$ species in the sewage sludge biocrude primarily begin at DBE 6, which corresponds to an indole core structure. In general, organic sediment-derived source material contains a more diverse population of nonbasic $N_1$ species relative to HTL biocrudes.

**$N_2$ Species.** The compositional space coverage of the basic $N_2$ species present within organic sediment-derived and biomass-derived materials can be seen in the (+) ESI FT-ICR mass spectra of GOM crude oil, shale oil, pine HTL biocrude, *Chlorella* sp. HTL biocrude, and sewage sludge HTL biocrude (Figure 5). The $N_2$ species present within the GOM crude oil range from $C_{27}$−$C_{75}$ and DBE 11-30 and account for ~3% the relative abundance of all the species present. Because the $N_2$ species start at a high DBE value (DBE 11), these species are most likely diaromatic.[32] Alternatively, the compositional space coverage of the shale oil ranges from $C_{15}$−$C_{59}$ and DBE 3-18. The $N_2$ species within the shale oil at DBE 3 correspond to imidazole structures, whereas the species at DBE 6 correspond to benzimidazole or azaindole structures.[34,32,33] However, the most abundant $N_2$ species present within the shale oil have a DBE value of 8 and do not fit into the "core plus additional benzene rings" motif. It is possible that these species contain 2 pyridinic nitrogen rings separated by an alkyl chain, which would account for a DBE value of 8, but further analysis would be needed to confirm.

The outlines of the organic sediment-derived $N_2$ species have been overlaid on the isoabundance-contoured plots of DBE vs carbon number for the members of the $N_2$ class derived from the (+) ESI FT-ICR mass spectra of the pine, *Chlorella* sp., and sewage sludge HTL biocrudes (Figure 5) to show the difference in compositional space coverage. The $N_2$ species within the pine HTL biocrude range from $C_{15}$−$C_{30}$ and DBE 6-17 and account for <0.3% of the relative abundance of all the species present. The most abundant species within the pine biocrude match for azacarbazole or dibenzimidazole structures (DBE 9). The *Chlorella* sp. and sewage sludge HTL biocrudes contain significantly more $N_2$ species than the pine biocrude due to the higher nitrogen contents of these feeds. The $N_2$ species within the *Chlorella* sp. and sewage sludge HTL biocrudes range from $C_{10}$−$C_{43}$ and DBE 3-22 and $C_{10}$−$C_{46}$ and DBE 3-25. Similar to the structures present within the shale oil, the *Chlorella* sp. and sewage sludge HTL biocrudes have


DOI: 10.1021/acs.energyfuels.6b03022
*Energy Fuels* 2017, 31, 2896−2906

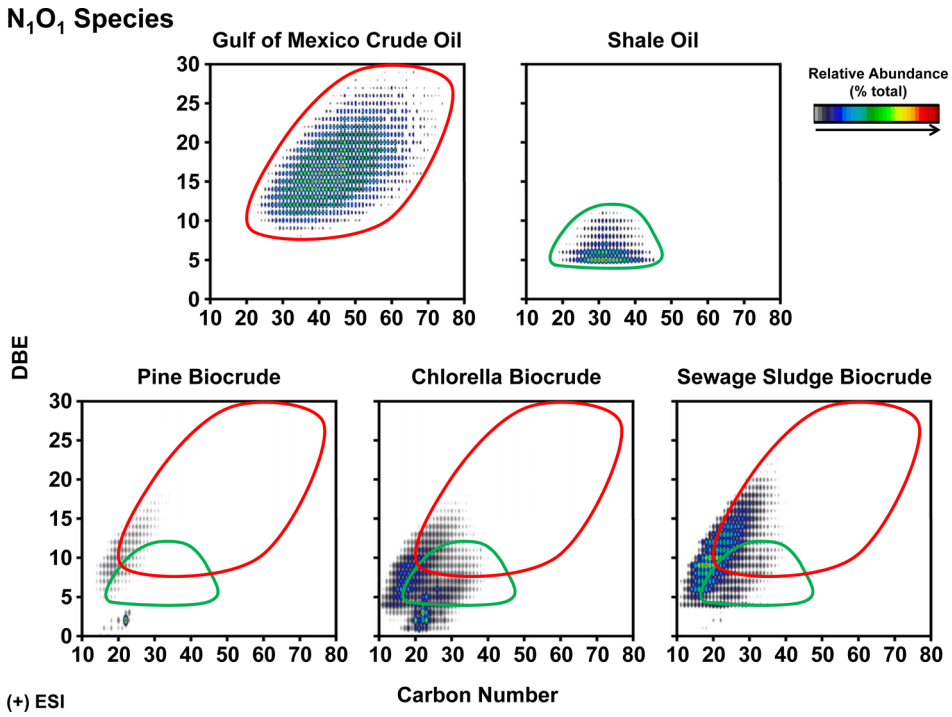


**Figure 7.** Isoabundance-contoured plots of double bond equivalents (DBE) versus carbon number for the $N_1O_1$ species derived from the (+) ESI mass spectra GOM crude oil, shale oil, pine HTL biocrude, *Chlorella* sp. HTL biocrude, and sewage sludge HTL biocrude.

structures that start with a DBE value of 3, which correspond to imidazole derivatives. Additional structures within the *Chlorella* sp. and sewage sludge biocrudes are representative of core structures with the addition of benzene rings at DBE 6 and 9 which correspond to benzimidazole/azaindole (or isomers) and dibenzimidazole/azacarbazole (or isomers) derivatives. The *Chlorella* sp. HTL biocrude also has abundant $N_2$ species that have a DBE value of 7, which match quinazoline/diazanapthalene derivatives and isomers. Similar to the trends seen in the $N_1$ species, the HTL biocrude $N_2$ species are apparently less alkylated and closer to the PAH line than the organic sediment-derived species.

The compositional space coverage of the nonbasic $N_2$ species present within organic sediment-derived and biomass-derived materials can be seen in the (−) ESI FT-ICR mass spectra of GOM of crude oil, shale oil, pine HTL biocrude, *Chlorella* sp. HTL biocrude, and sewage sludge HTL biocrude (Figure 6). The $N_2$ species within the GOM crude oil range from $C_{31}$−$C_{51}$ and DBE 14-23 and represent <0.3% of the relative abundance of all species ionized. Alternatively, the $N_2$ species in the shale oil range from $C_{13}$−$C_{59}$ and DBE 3-24 and represent ∼14% of the relative abundance of all the species ionized. Similar to positive-ion ESI, $N_2$ compounds with DBE values of 3, 6, and 9 are present and most likely correspond to imidazole, benzoimidazole/azaindole, and dibenzoimidazole/azacarbazole derivatives and their isomers. Additionally, $N_2$ species with DBE values of 7 and 10 are abundant within the shale oil. Those DBE and carbon number possibilities would fit to two possible scenarios, one being quinazoline/diazanapthalene and benzoquinazoline/benzonapthyridine derivatives and the second being benzoimidazole/azaindole and dibenzoimidazole/azacarbazole derivatives with one point of unsaturation on the alkyl chains. The latter choice would appear most probable for this ionization mode, which requires deprotonation.

Again, the profile of the organic sediment-derived $N_2$ species has been overlaid on the isoabundance contoured plots of DBE vs carbon number for the $N_2$ species from the pine, *Chlorella* sp., and sewage sludge HTL biocrudes to show a comparison of the compositional space coverage. No $N_2$ species within the pine biocrude were ionized by negative-ion ESI. The $N_2$ species present within the *Chlorella* sp. and sewage sludge biocrudes range from $C_{10}$−$C_{29}$ and DBE 3-14 and $C_{10}$−$C_{30}$ and DBE 6-17. The relative abundance profile of the $N_2$ species ionized by negative-ion ESI is very similar to the relative abundance profile seen in the $N_2$ species ionized by positive-ion ESI. Additionally, the $N_2$ species ionized by negative-ion ESI appear to cover the same compositional space as the most abundant species ionized by positive-ion ESI, which have less aromaticity and less alkylation. Furthermore, the abundant $N_2$ species have DBE values of 6 and 9, which most likely belong to benzoimidazole/azaindole and dibenzoimidazole/azacarbazole derivatives which have both pyridinic and pyrrolic nitrogen rings making the molecules susceptible to both protonation and deprotonation. From these observations, the $N_2$ species within the *Chlorella* sp. and sewage sludge HTL biocrudes ionized by negative-ion ESI are most likely the same species ionized by positive-ion ESI; however, negative-ion ESI only ionizes the smaller, less aromatic and alkylated compounds. This is dissimilar to the overall trend apparent between the $N_2$ species within the shale oil ionized by positive- and negative-ion ESI. Although there is compositional overlap between the $N_2$ species ionized by both positive- and negative-ion ESI within the shale oil (i.e., it is possible that these are the same compounds), the abundant species from each mode appear at different carbon number and DBE values, which points to the preferential ionization of different isomers based upon the ionization mode employed.

**$N_1O_1$ Species.** The compositional space coverage of the basic $N_1O_1$ species present within organic sediment-derived and biomass-dervied materials can be seen in the (+) ESI FT-



DOI: 10.1021/acs.energyfuels.6b03022
*Energy Fuels* 2017, 31, 2896−2906

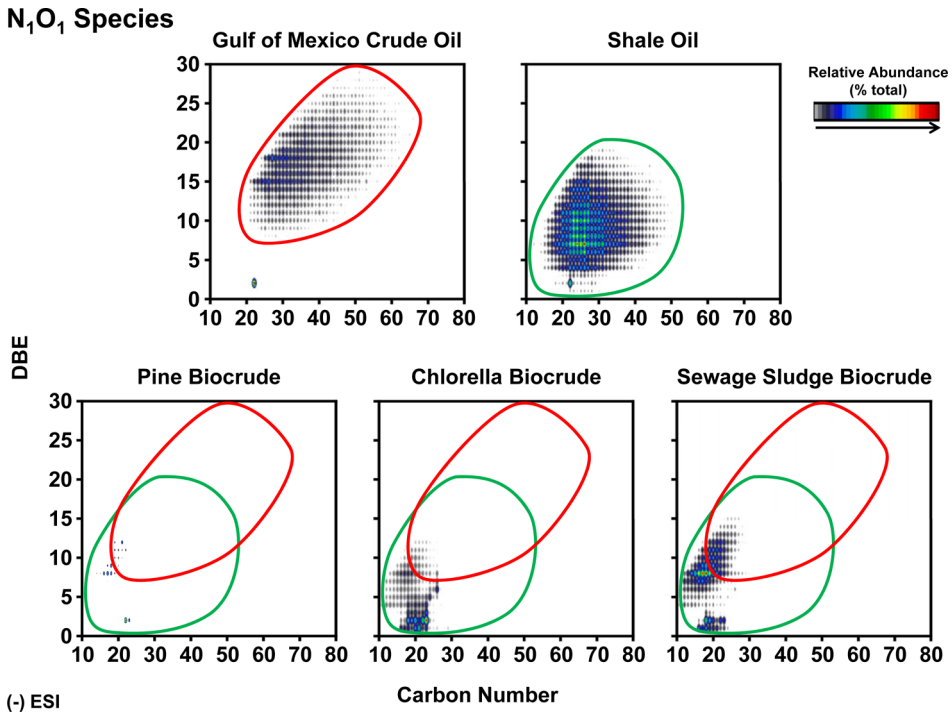


**Figure 8.** Isoabundance-contoured plots of double bond equivalents (DBE) versus carbon number for the $N_1O_1$ species derived from the (−) ESI mass spectra GOM crude oil, shale oil, pine HTL biocrude, *Chlorella* sp. HTL biocrude, and sewage sludge HTL biocrude.

ICR mass spectra of GOM crude oil, shale oil, pine HTL biocrude, *Chlorella* sp. HTL biocrude, and sewage sludge HTL biocrude (Figure 7). The $N_1O_1$ species within the GOM crude oil range from $C_{22}$−$C_{74}$ and DBE 8-30, whereas the $N_1O_1$ species within the shale oil range from $C_{19}$−$C_{46}$ and DBE 5-11. The $N_1O_1$ species within the shale oil have similar carbon number and abundance profiles as the abundant $N_1$ species from the shale oil, except the $N_1O_1$ species are one DBE higher than the $N_1$ species. Previous characterization of nitrogen−oxygen species from crude oil has shown the presence of IR absorption bands in the amide region.[32,33] Therefore, the $N_1O_1$ species within the shale oil most likely have the same core structures as the $N_1$ species with the addition of a carbonyl group to the pyridinic ring. However, other compositional isomers are possible. This trend of the addition of 1 DBE to the abundant $N_1$ species is not as apparent in the GOM crude oil; however, it is still present. The $N_1O_1$ species start at DBE 8, one DBE higher than the $N_1$ quinoline derivatives, and share similar compositional space as the $N_1$ species from the GOM crude oil.

The profile of the organic sediment-derived $N_1O_1$ species has been overlaid on the positive-ion ESI isoabundance contoured plots of DBE vs carbon number for the $N_1O_1$ species from the pine, *Chlorella* sp., and sewage sludge HTL biocrudes to show a comparison of the compositional space coverage. The $N_1O_1$ species within the pine, *Chlorella* sp., and sewage sludge HTL biocrudes range from $C_{13}$−$C_{34}$ and DBE 0-18, $C_{10}$-$C_{42}$ and DBE 0-18, and $C_{10}$-$C_{40}$ and DBE 1-22. All three biocrudes have $N_1O_1$ species below DBE 4, which most likely are amide structures (0 < DBE < 4).[35] Several compounds within the pine and *Chlorella* sp. biocrudes have a DBE value of 0 and must contain nitrogen and oxygen functionalities which do not contain a double bond (e.g., amine and alcohol/ether). The aromatic $N_1O_1$ species within the HTL biocrudes do not appear to follow the same trend as the organic sediment-derived compounds (i.e., addition of carbonyl to pyridinic ring structure) since the abundant aromatic compounds start at DBE 4 and there is not a noticeable increase in DBE from the $N_1$ species. Therefore, the $N_1O_1$ species within the HTL biocrudes most likely have different, dominant oxygen functionalities (e.g., alcohols or furans) than organic sediment-derived species. For example, the abundant species at DBE 6 and 9 could correspond to furopyridine and benzofuropyridine derivatives. However, multiple isomers are likely represented by the basic $N_1O_1$ species within HTL biocrudes, which have lower carbon numbers and DBE values than the GOM crude oil and shale oil $N_1O_1$ species.

The compositional space coverage of the nonbasic $N_1O_1$ species present within organic sediment-derived and biomass-derived materials can be seen in the (−) ESI FT-ICR mass spectra of GOM crude oil, shale oil, pine HTL biocrude, *Chlorella* sp. HTL biocrude, and sewage sludge HTL biocrude (Figure 8). The $N_1O_1$ species with the GOM crude oil range from $C_{13}$−$C_{68}$ and DBE 7-30, whereas the species within the shale oil range from $C_{12}$−$C_{52}$ and DBE 1-19. The nonbasic $N_1O_1$ species within the GOM crude oil have abundant compounds at DBE 15 and DBE 18, which correspond to benzene analogs of furopyridine. The shale oil has lower abundant species below DBE 4, which correspond to nonaromatic amide structures. The aromatic $N_1O_1$ species start at DBE 4 and have a "hot spot" at DBE 7 (i.e., addition of 3 DBE or benzene ring), which could correspond to a carbonyl addition to pyrrole and indole structures. However, other nitrogen- and oxygen-containing isomers likely contribute to the $N_1O_1$ species within the shale oil.

The profile of the organic sediment-derived $N_1O_1$ species has been overlaid on the positive-ion ESI isoabundance contoured plots of DBE vs carbon number for the nonbasic $N_1O_1$ species from the pine, *Chlorella* sp., and sewage sludge HTL biocrudes to show a comparison of the compositional space coverage.


DOI: 10.1021/acs.energyfuels.6b03022
*Energy Fuels* 2017, 31, 2896−2906

Unlike the $N_1O_1$ species ionized by positive-ion ESI, the species from the HTL biocrudes ionized by negative-ion ESI lie within the compositional space coverage of the organic sediment-derived species (mostly within the compositional space of the shale oil). The pine biocrude has very few $N_1O_1$ species which range from $C_8$−$C_{13}$ and DBE 2-12. The *Chlorella* sp. and sewage sludge biocrudes have more $N_1O_1$ species which range from $C_8$−$C_{29}$ and DBE 1-12 and $C_8$−$C_{30}$ and DBE 1-15. Both the *Chlorella* sp. and sewage sludge biocrudes have two distinct distributions of $N_1O_1$ species, the nonaromatic species (DBE < 4) and the aromatic species (DBE ≥ 4). The nonaromatic species most likely correspond to amide species, whereas the aromatic species probably contain a combination of different nitrogen and oxygen functionalities (e.g., pyrrole, hydroxyl, carbonyl, and furan). The most abundant species within all three HTL biocrudes have a DBE value of 8, which is consistent with that of furoindole derivatives.

**$O_x$ Species.** The crude oils from organic sediment-derived sources do not have significant contributions of $O_x$ species. The $O_x$ species that are present within the GOM crude oil and shale oil are mainly ionized by negative-ion ESI and contain either 1 or 2 oxygen atoms per molecule. The $O_1$ species present within the GOM crude oil range from $C_{14}$−$C_{63}$ and DBE 4-23, whereas the $O_2$ species range from $C_8$−$C_{58}$ and DBE 1-19. The $O_x$ species within the shale oil cover a slightly smaller compositional space with the $O_1$ species ranging from $C_{12}$−$C_{48}$ and DBE 1-17 and the $O_2$ species ranging from $C_{14}$−$C_{41}$ and DBE 1-13. Most of the organic sediment-derived $O_x$ species are aromatic (DBE > 3) and most likely contain phenol and furan functionalities.[32,33] However, the organic sediment-derived oils contain a series of fatty acids at DBE 1 which range from approximately $C_{14}$−$C_{32}$.

The HTL biocrudes, on the other hand, have significantly more $O_x$ species than the organic sediment-derived oils. The pine biocrude, which contains the highest oxygen content, has the most diverse $O_x$ population with molecules containing up to 8 oxygen atoms. Most of the $O_x$ species within the pine biocrude are aromatic (DBE > 3) and contain a variety of oxygen functionalities (e.g., phenols, methoxyphenols, furans). Compositionally, the species within each $O_x$ class cover a smaller carbon number range (i.e., less alkylation) for any given DBE than the organic sediment-derived oils. Additionally, the carbon number of the $O_x$ species within the biocrudes increase as DBE increases (i.e., compositional space contains linear slope), unlike petroleum in which the carbon number range stays fairly consistent with increasing DBE (i.e., circular compositional space).

The *Chlorella* sp. and sewage sludge biocrudes have a less diverse $O_x$ population and range from $O_1$−$O_4$ and $O_1$−$O_5$. These two biocrudes contain <30 $O_1$ species, whereas the pine biocrude contains 130 $O_1$ species and the organic sediment-derived oils contain >350 $O_1$ compounds. This suggests that the *Chlorella* sp. and sewage sludge biocrudes contain different structures (which contain multiple oxygen atoms) than the dominant phenolic and furan species that comprise the $O_1$ class within the pine biocrude and organic sediment-derived oils. Most of the $O_x$ species within the *Chlorella* sp. and sewage sludge biocrudes are aliphatic carboxylic ($O_2$, 34% and 21%) and hydroxy ($O_3$, 3% and 5%) acids, although the sewage sludge biocrude contains some lower abundant aromatic species (DBE > 3). Unlike the aliphatic acids in organic sediment-derived oils which mainly contain saturated fatty acids (DBE = 1), the acids within the biocrudes range from $C_{12}$−$C_{28}$ and DBE 1-7. The predominant acids within the biocrudes contain 16 or 18 carbons and range from DBE 1-4, whereas the most abundant acids within the organic sediment-derived oils are $C_{22}$, DBE = 2 species.

## CONCLUSION

Generally, GOM crude oil and shale oil are dominated by pure hydrocarbons and nitrogen-containing species, whereas HTL biocrudes are dominated by oxygen-containing species. Biocrudes can have >15 heteroatoms per molecule, and this heteroatom complexity exceeds that of the crude and shale oils. Also, HTL biocrudes contain abundant, low carbon number compounds and have less alkylation per core structure (i.e., fewer carbon numbers represented for any given DBE value) than either the GOM crude oil or the shale oil. HTL biocrudes are more compositionally similar to shale oil than the more mature, GOM crude oil.

These analyses suggest that HTL oils will behave quite differently than crude oil in a refinery process. Refinement of HTL biocrudes will generate smaller compounds with fewer carbon numbers per core structure compared to organic sediment-derived oils. HTL biocrudes will require deoxygenation and/or denitrogenation before their composition and behavior are similar to organic sediment-derived oils.

Most interesting, the composition of the *Chlorella* sp. and sewage sludge biocrudes is very similar, which suggests sewage sludge biocrudes as an extremely cost-effective substitute for algal-derived biocrudes. Generation of sewage sludge biocrudes from wastewater treatment plants would captialize on the high cost of WWTP solid waste disposal (i.e., up to $300/ton) to mitigate biocrude production cost, whereas current algal feedstock costs exceed $1000/dry ton.[36] Finally, sewage sludge biocrude has a lower iron content than the *Chlorella* sp. biocrude (Table S1), which has been shown to be detrimental to biocrude upgrading processes.[20]

## ASSOCIATED CONTENT

### Supporting Information

The Supporting Information is available free of charge on the ACS Publications website at DOI: 10.1021/acs.energyfuels.6b03022. .

Figures S1 and S2 and Table S1 (PDF)

## AUTHOR INFORMATION

### Corresponding Author

*Phone: +1 575 646 5156. Fax: +1 575 646 1597. E-mail: tschaub@nmsu.edu.

### ORCID

Tanner M. Schaub: 0000-0002-5747-4237

### Notes

The authors declare no competing financial interest.

## ACKNOWLEDGMENTS

This work was supported by the U.S. Department of Energy's Office of Energy Efficiency and Renewable Energy (Bioenergy Technologies Office), the United States National Science Foundation (IIA-1301346), the Center for Animal Health and Food Safety at New Mexico State University, and NSF Division of Materials Research (DMR-11-57490). The authors would like to thank the ICR staff at National High Magnetic Field for



DOI: 10.1021/acs.energyfuels.6b03022
Energy Fuels 2017, 31, 2896−2906

the use of the FT-ICR MS facility and assistance with instrument configuration and data collection.

## REFERENCES

(1) Behrendt, F.; Neubauer, Y.; Oevermann, M.; Wilmes, B.; Zobel, N. *Chem. Eng. Technol.* **2008**, *31* (5), 667−677.
(2) Toor, S. S.; Rosendahl, L.; Rudolf, A. *Energy* **2011**, *36* (5), 2328−2342.
(3) Elliott, D. C.; Biller, P.; Ross, A. B.; Schmidt, A. J.; Jones, S. B. *Bioresour. Technol.* **2015**, *178*, 147−156.
(4) Elliott, D. C.; Hart, T. R.; Schmidt, A. J.; Neuenschwander, G. G.; Rotness, L. J.; Olarte, M. V.; Zacher, A. H.; Albrecht, K. O.; Hallen, R. T.; Holladay, J. E. *Algal Res.* **2013**, *2* (4), 445−454.
(5) Marshall, A. G.; Rodgers, R. P. *Acc. Chem. Res.* **2004**, *37* (1), 53−59.
(6) Schaub, T. M.; Jennings, D. W.; Kim, S.; Rodgers, R. P.; Marshall, A. G. *Energy Fuels* **2007**, *21* (1), 185−194.
(7) Purcell, J. M.; Merdrignac, I.; Rodgers, R. P.; Marshall, A. G.; Gauthier, T.; Guibard, I. *Energy Fuels* **2010**, *24* (4), 2257−2265.
(8) Lobodin, V. V.; Nyadong, L.; Ruddy, B. M.; Curtis, M.; Jones, P. R.; Rodgers, R. P.; Marshall, A. G. *Int. J. Mass Spectrom.* **2015**, *378*, 186.
(9) Faeth, J. L.; Jarvis, J. M.; McKenna, A. M.; Savage, P. E. *AIChE J.* **2016**, *62*, 815.
(10) Lobodin, V. V.; Robbins, W. K.; Lu, J.; Rodgers, R. P. *Energy Fuels* **2015**, *29* (10), 6177−6186.
(11) Corilo, Y. E.; Rowland, S. M.; Rodgers, R. P. *Energy Fuels* **2016**, *30*, 3962.
(12) Juyal, P.; Mapolelo, M. M.; Yen, A.; Rodgers, R. P.; Allenson, S. J. *Energy Fuels* **2015**, *29* (4), 2342−2350.
(13) Sudasinghe, N.; Dungan, B.; Lammers, P.; Albrecht, K.; Elliott, D.; Hallen, R.; Schaub, T. *Fuel* **2014**, *119*, 47−56.
(14) Sudasinghe, N.; Cort, J. R.; Hallen, R.; Olarte, M.; Schmidt, A.; Schaub, T. *Fuel* **2014**, *137*, 60−69.
(15) Reddy, H. K.; Muppaneni, T.; Ponnusamy, S.; Sudasinghe, N.; Pegallapati, A.; Selvaratnam, T.; Seger, M.; Dungan, B.; Nirmalakhandan, N.; Schaub, T. *Appl. Energy* **2016**, *165*, 943−951.
(16) Sanguineti, M. M.; Hourani, N.; Witt, M.; Sarathy, S. M.; Thomsen, L.; Kuhnert, N. *Algal Res.* **2015**, *9*, 227−235.
(17) Speight, J. G. *Handbook of petroleum analysis*; Winefordner, J. D., Ed.; Chemical analysis; Wiley-Interscience: New York, NY, 2001.
(18) Liu, T.; Lu, J.; Zhao, X.; Zhou, Y.; Wei, Q.; Xu, C.; Zhang, Y.; Ding, S.; Zhang, T.; Tao, X.; Ju, L.; Shi, Q. *Energy Fuels* **2015**, *29* (4), 2089−2096.
(19) Rodgers, R. P.; Hendrickson, C. L.; Emmett, M. R.; Marshall, A. G.; Greaney, M.; Qian, K. *Can. J. Chem.* **2001**, *79* (5−6), 546−551.
(20) Jarvis, J. M.; Sudasinghe, N. M.; Albrecht, K. O.; Schmidt, A. J.; Hallen, R. T.; Anderson, D. B.; Billing, J. M.; Schaub, T. M. *Fuel* **2016**, *182*, 411−418.
(21) Snowden-Swan, L.; Zhu, Y.; Jones, S.; Elliott, D.; Schmidt, A.; Hallen, R.; Billing, J.; Hart, T.; Fox, S.; Maupin, G. *Hydrothermal Liquefaction and Upgrading of Municipal Wastewater Treatment Plant Sludge: A Preliminary Techno-Economic Analysis*; Richland, WA, 2016.
(22) Marrone, P. A. *Genifuel Hydrothermal Processing Bench-Scale Technology Evaluation Project*; London, UK, 2016.
(23) Kaiser, N. K.; Quinn, J. P.; Blakney, G. T.; Hendrickson, C. L.; Marshall, A. G. *J. Am. Soc. Mass Spectrom.* **2011**, *22*, 1343−1351.
(24) Blakney, G. T.; Hendrickson, C. L.; Marshall, A. G. *Int. J. Mass Spectrom.* **2011**, *306* (306), 246−252.
(25) Senko, M. W.; Hendrickson, C. L.; Emmett, M. R.; Shi, S. D.-H.; Marshall, A. G. *J. Am. Soc. Mass Spectrom.* **1997**, *8*, 970−976.
(26) Kaiser, N. K.; Savory, J. J.; McKenna, A. M.; Quinn, J. P.; Hendrickson, C. L.; Marshall, A. G. *Anal. Chem.* **2011**, *83*, 6907−6910.
(27) Ledford, E. B., Jr.; Rempel, D. L.; Gross, M. L. *Anal. Chem.* **1984**, *56*, 2744−2748.
(28) Corilo, Y. E. *PetroOrg Software*. Florida State University. All rights reserved. www.petroorg.com (accessed Feb 13, 2017).
(29) Kendrick, E. *Anal. Chem.* **1963**, *35*, 2146−2154.
(30) Speight, J. G. *The Chemistry and Technology of Petroleum*, 4th ed.; Chemical Industries; CRC Press: 2006.
(31) Panisko, E.; Wietsma, T.; Lemmon, T.; Albrecht, K.; Howe, D. *Biomass Bioenergy* **2015**, *74*, 162−171.
(32) Snyder, L. R.; Buell, B. E.; Howard, H. E. *Anal. Chem.* **1968**, *40* (8), 1303−1317.
(33) Snyder, L. R. *Anal. Chem.* **1969**, *41* (2), 314−323.
(34) Chen, X.; Shen, B.; Sun, J.; Wang, C.; Shan, H.; Yang, C.; Li, C. *Energy Fuels* **2012**, *26* (3), 1707−1714.
(35) Chen, W.-T.; Tang, L.; Qian, W.; Scheppe, K.; Nair, K.; Wu, Z.; Gai, C.; Zhang, P.; Zhang, Y. *ACS Sustainable Chem. Eng.* **2016**, *4* (4), 2182−2190.
(36) Billing, J. M. Hydrothermal Liquefaction of Wastewater Treatment Plant Solids. *Task 34 Newsletter: Direct Thermochemical Liquefaction*; 2016; Issue 39, pp 17−18.



DOI: 10.1021/acs.energyfuels.6b03022
*Energy Fuels* 2017, 31, 2896−2906